Magazine of Civil Engineering

ISSN 2712-8172

journal homepage: http://engstroy.spbstu.ru/

Research article

UDC 539.3

DOI: 10.34910/MCE.141.9

Comparison of single-field and three-field fem in nonlinear shell calculations

M.Yu. Klochkov[1], ***V.A. Pshenichkina***[1], ***A.P. Nikolaev***[2], ***Yu.V. Klochkov***[2], ***O.V. Vakhnina***[2] ✉

[1] *Volgograd State Technical University, Volgograd, Russian Federation*

[2] *Volgograd State Agrarian University, Volgograd, Russian Federation*

✉ *ovahnina@bk.ru*

Keywords: three-field finite element method, nonlinear mixed functional, kinematic unknowns, force unknowns, deformation unknowns

Abstract. On the basis of physical equations of deformation theory of plasticity using Kirchhoff–Lava hypothesis, matrix dependences between columns of forces and moments and columns of deformations and curvatures of the shell midface are determined at the loading step. As a finite element, a quadrilateral fragment of the shell midface with nodal unknowns in the form of: increments of displacements and their derivatives; increments of deformations and increments of curvatures; increments of forces and increments of moments were used. To approximate the required quantities, the following expressions are adopted: bicubic functions with elements of Hermite polynomials of the third degree for displacements; bilinear functions for deformation and force parameters. To obtain the stiffness matrix of the finite element, the nonlinear Lagrangian functional on the loading step was used with an additional condition: the real work of the difference of forces determined using their direct approximation and using approximating expressions for displacements, on deformations and curvatures of the loading step must be equal to zero. Minimisation of the functional by nodal unknowns provides three systems of equations, the solution of which determines the stiffness matrix of the finite element used to calculate the displacement fields. The force and deformation parameters at the discretisation nodes of the shell are determined from the displacements found. Case studies show the effectiveness of using a three-field finite element method (FEM) technique compared to using FEM in the displacement method formulation (single-field technique).

Citation: Klochkov, M.Yu., Pshenichkina, V.A., Nikolaev, A.P., Klochkov, Yu.V., Vakhnina, O.V. Comparison of single-field and three-field fem in nonlinear shell calculations. Magazine of Civil Engineering. 2026. 19(1). Article no. 14109. DOI: 10.34910/MCE.141.9

1. Introduction

Definition of the object of study. Structures consisting of shells and their fragments are now increasingly used in various fields. These include hangars, warehouses, domes and slabs, tanks, bunkers, cisterns, pipelines and others. The worldwide trend aimed at significant reduction of material intensity of systems and objects actualises the problem of determining the stress-strain state (SSS) of structures in the form of shells and their fragments in a physically nonlinear formulation.

Assumption within the regulated limits of the plastic stage of the applied material of structures allows to reduce the overall material intensity of structures, including those consisting of shells.

Literature review. The developed theory of solid body deformation [1–4] turned out to be theoretically unrealisable in the practice of engineering calculations of real structures, which led to the development of numerical methods for solving the equations of solid body deformation mechanics [5–9]. At the present stage of development of structural mechanics and computer science, the main tool for investigating the SSS of shell structures beyond the elastic limit is numerical finite element method (FEM). In spite of the considerable volume of publications on this subject [10–15] and the availability of foreign (ANSYS, ABAQUS, NASTRAN, etc.) and domestic (PRIIS, LIRA, etc.) finite element computational systems, the problem of finding the most optimal formulations of the FEM for the calculation of shell structures in a physically nonlinear setting remains quite relevant. It is known that the FEM in the form of the displacement method is the most widespread at present, but it does not lack the disadvantages associated with the use of only one field of unknowns – the displacement field. The mixed variant of the FEM with kinematic and force fields of unknowns [16–23], as well as the FEM variant with three fields of unknowns [24, 25], are becoming the most promising.

Purpose and objectives of the study. In this paper, the three-field variant of the mixed FEM is applied to the calculation of shells under elastic-plastic deformation and the finite element solutions obtained on its basis are compared with the solutions obtained using the FEM in the formulation of the displacement method in a physically nonlinear setting.

2. Materials and Methods

In order to realise the three-field variant of the mixed FEM in a physically nonlinear formulation, it is first of all necessary to formulate the corresponding nonlinear three-field functional. For this purpose, we introduce the following matrix notations: $\underset{1\times6}{\left\{S^{\alpha\beta}\right\}^T}=\left\{N^{11}N^{22}N^{12}M^{11}M^{22}M^{12}\right\}$; $\underset{1\times6}{\left\{\Delta S^{\alpha\beta}\right\}^T}=\left\{\Delta N^{11}\Delta N^{22}\Delta N^{12}\Delta M^{11}\Delta M^{22}\Delta M^{12}\right\}$ is matrix-string of longitudinal forces and bending moments and their increments at the loading step, respectively; $\underset{1\times6}{\left\{\Delta\varepsilon_{\alpha\beta}\right\}^T}=\left\{\Delta\varepsilon_{11}\Delta\varepsilon_{22}2\Delta\varepsilon_{12}\Delta\aleph_{11}\Delta\aleph_{22}2\Delta\aleph_{12}\right\}$ is matrix-string of deformation increments and curvature increments at the midpoint of the shell structure surface at the loading step; $\underset{1\times3}{\left\{\Delta U\right\}^T}=\left\{\Delta v^1\Delta v^2\Delta v\right\}$ is matrix-string of step increments of displacement vector components; $\underset{1\times3}{\left\{P\right\}^T}=\left\{p_1p_2p\right\}$; $\underset{1\times3}{\left\{\Delta P\right\}^T}=\left\{\Delta p_1\Delta p_2\Delta p\right\}$ are matrix-string of external surface load vector components and their step increments, respectively.

The increments of longitudinal forces $\Delta N^{\alpha\beta}$ and increments of bending moments $\Delta M^{\alpha\beta}$ at the loading step can be expressed through the increments of deformation and increments of curvature $\left\{\Delta\varepsilon_{\alpha\beta}\right\}$ using the following relations:

$$\underset{3\times1}{\left\{\Delta N^{\alpha\beta}\right\}}=\int\limits_{-\frac{h}{2}}^{\frac{h}{2}}\left\{\Delta\sigma^{\alpha\beta}\right\}d\zeta=\int\limits_{-\frac{h}{2}}^{\frac{h}{2}}\underset{3\times3}{\left[C_p\right]}\underset{3\times6}{\left[G\right]}d\zeta\underset{6\times1}{\left\{\Delta\varepsilon_{\alpha\beta}\right\}}=\underset{3\times6}{\left[\alpha_p\right]}\underset{6\times1}{\left\{\Delta\varepsilon_{\alpha\beta}\right\}};\tag{1}$$

$$\underset{3\times1}{\left\{\Delta M^{\alpha\beta}\right\}}=\int\limits_{-\frac{h}{2}}^{\frac{h}{2}}\left\{\Delta\sigma^{\alpha\beta}\right\}\zeta d\zeta=\int\limits_{-\frac{h}{2}}^{\frac{h}{2}}\underset{3\times3}{\left[C_p\right]}\underset{3\times6}{\left[G\right]}\zeta d\zeta\underset{6\times1}{\left\{\Delta\varepsilon_{\alpha\beta}\right\}}=\underset{3\times6}{\left[\beta_p\right]}\underset{6\times1}{\left\{\Delta\varepsilon_{\alpha\beta}\right\}},\tag{2}$$

where $\underset{1\times3}{\left\{\Delta N^{\alpha\beta}\right\}^T}=\left\{\Delta N^{11}\Delta N^{22}\Delta N^{12}\right\}$; $\underset{1\times3}{\left\{\Delta M^{\alpha\beta}\right\}^T}=\left\{\Delta M^{11}\Delta M^{22}\Delta M^{12}\right\}$; $\underset{3\times6}{\left[\alpha_p\right]}=\int\limits_{-\frac{h}{2}}^{\frac{h}{2}}\underset{3\times3}{\left[C_p\right]}\underset{3\times6}{[G]}d\zeta$ and $\underset{3\times6}{\left[\beta_p\right]}=\int\limits_{-\frac{h}{2}}^{\frac{h}{2}}\underset{3\times3}{\left[C_p\right]}\underset{3\times6}{[G]}\zeta d\zeta$ are matrices obtained by numerically finding definite integrals; $\underset{1\times3}{\left\{\Delta\sigma^{\alpha\beta}\right\}^T}=\left\{\Delta\sigma^{11}\Delta\sigma^{22}\Delta\sigma^{12}\right\}$ are the increments of the contravariant components of the stress tensor at the loading step.

The plasticity matrix included in (1) and (2) $\left[C_p\right]$ is composed on the basis of the relationships of the deformation theory of plasticity [4], represented in a curvilinear coordinate system by the expression:

$$E_{\alpha\beta}=\frac{3}{2}\cdot\frac{\varepsilon_i}{\sigma_i}T_{\alpha\beta}, \tag{3}$$

where $E_{\alpha\beta}=\varepsilon^{\varsigma}_{\alpha\beta}-\frac{1}{3}g_{\alpha\beta}P_{\varepsilon}$ are components of the deformation deviator; ε_i, σ_i are intensity of deformations and stresses; $T_{\alpha\beta}=\sigma_{\alpha\beta}-\frac{1}{3}g_{\alpha\beta}P_{\sigma}$ is stress deviator; $P_{\varepsilon}=g^{\alpha\beta}\varepsilon_{\alpha\beta}$, $P_{\sigma}=g_{\mu\nu}\sigma^{\mu\nu}$ are first invariants of strain and stress tensors; $g_{\alpha\beta}$, $g^{\alpha\beta}$ are covariant and contravariant components of the metric tensor.

The increments of deformations in an arbitrary layer at a loading step are determined by differentiating (3) in the following general form:

$$\Delta\varepsilon^{\varsigma}_{\alpha\beta}=\frac{\partial\varepsilon^{\varsigma}_{\alpha\beta}}{\partial\sigma^{\mu\nu}}\Delta\sigma^{\mu\nu}. \tag{4}$$

The partial derivatives included in (4) were determined by the relations:

$$\begin{aligned}\frac{\partial\varepsilon^{\varsigma}_{11}}{\partial\sigma^{11}}&=\frac{3}{2}\cdot\frac{\varepsilon_i}{\sigma_i}g_{11}g_{11}+\frac{3}{2}\left(g_{11}g_{11}\sigma^{11}+2g_{11}g_{12}\sigma^{12}+g_{12}g_{12}\sigma^{22}\right)\cdot\frac{\partial\left(\varepsilon_i/\sigma_i\right)}{\partial\sigma^{11}}+\\&+g_{11}g_{11}\left(\frac{1}{3}\cdot\frac{1-2\nu}{E}-\frac{1}{2}\cdot\frac{\varepsilon_i}{\sigma_i}\right)-\frac{1}{2}g_{11}P_{\sigma}\cdot\frac{\partial\left(\varepsilon_i/\sigma_i\right)}{\partial\sigma^{11}};\\\frac{\partial\varepsilon^{\varsigma}_{12}}{\partial\sigma^{12}}&=\frac{3}{2}\cdot\frac{\varepsilon_i}{\sigma_i}\left(g_{12}g_{22}+g_{12}g_{21}\right)+\\&+\frac{3}{2}\left(g_{11}g_{21}\sigma^{11}+\sigma^{12}\left(g_{11}g_{22}+g_{12}g_{21}\right)+g_{12}g_{22}\sigma^{22}\right)\cdot\frac{\partial\left(\varepsilon_i/\sigma_i\right)}{\partial\sigma^{12}}+\\&+2g_{12}g_{12}\left(\frac{1}{3}\cdot\frac{1-2\nu}{E}-\frac{1}{2}\cdot\frac{\varepsilon_i}{\sigma_i}\right)-\frac{1}{2}g_{12}P_{\sigma}\cdot\frac{\partial\left(\varepsilon_i/\sigma_i\right)}{\partial\sigma^{12}},\end{aligned} \tag{5}$$

where E is modulus of elasticity; ν is coefficient of transverse deformation.

The derivatives of the ratio of strain and stress intensities included in (5) are determined by the expressions:

$$\frac{\partial\left(\varepsilon_i/\sigma_i\right)}{\partial\sigma^{\mu\tau}}=\frac{\partial\left(\varepsilon_i/\sigma_i\right)}{\partial\sigma_i}\cdot\frac{\partial\sigma_i}{\partial\sigma^{\mu\tau}}=\left(\frac{\partial\varepsilon_i}{\partial\sigma_i}\sigma_i-1\cdot\varepsilon_i\right)\cdot\frac{1}{\sigma_i^2}=\psi\frac{\partial\sigma_i}{\partial\sigma^{\mu\tau}},\tag{6}$$

where $\psi=\frac{1}{\sigma_i}\left(\frac{1}{E_K}-\frac{1}{E_C}\right)$; E_K, E_C are tangent and secant modules of the deformation diagram;

$$\frac{\partial\sigma_i}{\partial\sigma^{11}}=\frac{3}{4}\cdot\frac{1}{\sigma_i}\left(\left(1-\frac{1}{3}g^{11}g_{11}\right)T_{11}+\frac{2}{3}g_{11}g_{11}T^{11}-\frac{1}{3}g^{22}g_{11}T_{22}+\right.$$

$$\left.+\left(g_{21}g_{21}-\frac{1}{3}g_{22}g_{11}\right)T^{22}-\frac{2}{3}g^{12}g_{11}\right)T_{12}+\frac{4}{3}g_{11}g_{21}T^{12}-\frac{1}{3}g^{33}g_{11}T_{33}-\frac{1}{3}g_{33}g_{11}T^{33}.$$

Using (4), (5), (6) a matrix dependence is formed:

$$\underset{3\times1}{\left\{\Delta\varepsilon\right\}}=\underset{3\times3}{\left[\omega\right]}\underset{3\times1}{\left\{\Delta\sigma^{\alpha\beta}\right\}},\tag{7}$$

where $\underset{1\times3}{\left\{\Delta\varepsilon^{\varsigma}\right\}^T}=\left\{\Delta\varepsilon_{11}^{\varsigma}\Delta\varepsilon_{22}^{\varsigma}2\Delta\varepsilon_{12}^{\varsigma}\right\}$.

Matrix $\underset{3\times3}{\left[C_p\right]}$ determined by matrix inversion $\underset{3\times3}{\left[\omega\right]}$.

Taking into account the above, the matrix relationship is written:

$$\underset{3\times1}{\left\{\Delta\sigma^{\alpha\beta}\right\}}=\underset{3\times3}{\left[C_p\right]}\underset{3\times1}{\left\{\Delta\varepsilon_{\alpha\beta}^{\zeta}\right\}}=\underset{3\times3}{\left[C_p\right]}\underset{3\times6}{\left[G\right]}\underset{6\times1}{\left\{\Delta\varepsilon_{\alpha\beta}\right\}},\tag{8}$$

where $\underset{1\times3}{\left\{\Delta\varepsilon_{\alpha\beta}^{\zeta}\right\}^T}=\left\{\Delta\varepsilon_{11}^{\zeta}\Delta\varepsilon_{22}^{\zeta}2\Delta\varepsilon_{12}^{\zeta}\right\}$; $\underset{3\times6}{\left[G\right]}=\begin{bmatrix}1&0&0&\zeta&0&0\\0&1&0&0&\zeta&0\\0&0&1&0&0&\zeta\end{bmatrix}$.

Taking into account (1) and (2), the following matrix relation can be composed as follows:

$$\underset{6\times1}{\left\{\Delta S_K^{\alpha\beta}\right\}}=\underset{6\times6}{\left[\gamma\right]}\underset{6\times1}{\left\{\Delta\varepsilon_{\alpha\beta}\right\}},\tag{9}$$

where $\underset{6\times6}{\left[\gamma\right]}=\begin{bmatrix}\underset{3\times6}{\left[\alpha_p\right]}\\\underset{3\times6}{\left[\beta_p\right]}\end{bmatrix}$.

If we use a four-node fragment of its midface [24] with nodes i, j, k, l as a discretisation element of the shell structure, the increments of longitudinal forces and increments of bending moments at the loading step can be expressed through their nodal values by means of bilinear relationships:

$$\Delta Q^{\alpha\beta}=\frac{1-\xi}{2}\cdot\frac{1-\eta}{2}\left(\Delta Q^{\alpha\beta}\right)^i+\frac{1+\xi}{2}\cdot\frac{1-\eta}{2}\left(\Delta Q^{\alpha\beta}\right)^j+\frac{1+\xi}{2}\cdot\frac{1+\eta}{2}\left(\Delta Q^{\alpha\beta}\right)^k+$$
$$+\frac{1-\xi}{2}\cdot\frac{1+\eta}{2}\left(\Delta Q^{\alpha\beta}\right)^l=\underset{1\times4}{\left\{\varphi\right\}^T}\underset{1\times4}{\left\{\Delta Q_u^{\alpha\beta}\right\}},\tag{10}$$

where $-1 \le \xi,\ \eta \le 1$ are local coordinates used to organise the procedure of numerical integration by Gauss quadrature; $\underset{1\times4}{\left\{\Delta Q_u^{\alpha\beta}\right\}^T} = \left\{\left(\Delta Q^{\alpha\beta}\right)^i \left(\Delta Q^{\alpha\beta}\right)^j \left(\Delta Q^{\alpha\beta}\right)^k \left(\Delta Q^{\alpha\beta}\right)^l\right\}$.

Here, $\Delta Q^{\alpha\beta}$ is understood as $\Delta N^{\alpha\beta}$ or $\Delta M^{\alpha\beta}$. On the basis of (10), a matrix dependence can be compiled:

$$\underset{6\times1}{\left\{\Delta S_a^{\alpha\beta}\right\}} = \underset{6\times24}{\left[H\right]} \underset{24\times1}{\left\{\Delta S_u^{\alpha\beta}\right\}}, \tag{11}$$

where $\underset{6\times24}{\left[H\right]}$ is a quasi-diagonal matrix, on the main diagonal of which the row matrices $\underset{1\times4}{\left\{\varphi\right\}^T}$; $\underset{1\times24}{\left\{\Delta S_u^{\alpha\beta}\right\}^T} = \left\{\underset{1\times12}{\left\{\Delta N_u^{\alpha\beta}\right\}^T} \quad \underset{1\times12}{\left\{\Delta M_u^{\alpha\beta}\right\}^T}\right\}$.

Taking into account the notations introduced above and (1)–(11), the nonlinear mixed functional can be written in the following form:

$$\begin{aligned}\Phi_S = \int_F \left[\underset{1\times6}{\left\{S^{\alpha\beta}\right\}^T} + \frac{1}{2}\underset{1\times6}{\left\{\Delta S_a^{\alpha\beta}\right\}^T}\right] \underset{6\times1}{\left\{\Delta\varepsilon_{\alpha\beta a}\right\}} dF - \\ - \int_F \underset{1\times3}{\left\{\Delta U\right\}^T} \left[\underset{3\times1}{\left\{P\right\}} + \frac{1}{2}\underset{3\times1}{\left\{\Delta P\right\}}\right] dF + \frac{1}{2}\int_F \left[\underset{1\times6}{\left\{\Delta S_K^{\alpha\beta}\right\}^T} - \underset{1\times6}{\left\{\Delta S_a^{\alpha\beta}\right\}^T}\right] \underset{6\times1}{\left\{\Delta\varepsilon_{\alpha\beta a}\right\}} dF.\end{aligned} \tag{12}$$

The column of increments of deformations and curvatures of the medial surface of the shell structure included in (12) can be expressed similarly to (11) through their nodal values:

$$\underset{6\times1}{\left\{\Delta\varepsilon_{\alpha\beta a}\right\}} = \underset{6\times24}{\left[H\right]} \underset{24\times1}{\left\{\Delta\varepsilon_{\alpha\beta u}\right\}}, \tag{13}$$

and can be represented by the Cauchy relations for thin shells [26] by a matrix product:

$$\underset{6\times1}{\left\{\Delta\varepsilon_{\alpha\beta K}\right\}} = \underset{6\times3}{\left[D\right]} \underset{3\times1}{\left\{\Delta U\right\}}. \tag{14}$$

The column of step increments of the components of the displacement vector of a point of the centre surface of the shell structure can be interpolated through the nodal values of the component increments by means of products of Hermite polynomials of the third degree:

$$\underset{3\times1}{\left\{\Delta U\right\}} = \underset{3\times36}{\left[A\right]} \underset{36\times1}{\left\{\Delta U^L\right\}} = \underset{3\times36}{\left[A\right]} \underset{36\times36}{\left[P_R\right]} \underset{36\times1}{\left\{\Delta U^G\right\}}, \tag{15}$$

where $\underset{3\times36}{\left[A\right]}$ is a quasi-diagonal matrix containing matrix-rows of polynomial Hermite functions; $\underset{36\times1}{\left\{\Delta U^L\right\}}$ and $\underset{36\times1}{\left\{\Delta U^G\right\}}$ are columns of kinematic nodal unknowns at the loading step in local and global coordinate systems, respectively, and $\underset{36\times36}{\left[P_R\right]}$ is the transition matrix from column $\underset{36\times1}{\left\{\Delta U^L\right\}}$ to column $\underset{36\times1}{\left\{\Delta U^G\right\}}$.

The relation (14) taking into account (15) will take the form:

$$\underset{6\times1}{\left\{\Delta\varepsilon_{\alpha\beta K}\right\}} = \underset{6\times3}{\left[D\right]} \underset{3\times36}{\left[A\right]} \underset{36\times36}{\left[P_R\right]} \underset{36\times1}{\left\{\Delta U^G\right\}} = \underset{6\times36}{\left[B\right]} \underset{36\times36}{\left[P_R\right]} \underset{36\times1}{\left\{\Delta U^G\right\}}, \tag{16}$$

where $\underset{1\times36}{\left\{\Delta U^L\right\}^T}=\left\{\underset{1\times12}{\left\{\Delta v^{1L}\right\}^T}\ \underset{1\times12}{\left\{\Delta v^{2L}\right\}^T}\ \underset{1\times12}{\left\{\Delta v^{L}\right\}^T}\right\}$; $\underset{1\times36}{\left\{\Delta U^G\right\}^T}=\left\{\underset{1\times12}{\left\{\Delta v^{1G}\right\}^T}\ \underset{1\times12}{\left\{\Delta v^{2G}\right\}^T}\ \underset{1\times12}{\left\{\Delta v^{G}\right\}^T}\right\}$;

$$\underset{1\times12}{\left\{\Delta q^L\right\}^T}=\left\{\Delta q^i\ \ \Delta q^j\ \ \Delta q^k\ \ \Delta q^l\ \ \Delta q^i_{,\xi}\dots\Delta q^l_{,\xi}\ \ \Delta q^i_{,\eta}\dots\Delta q^l_{,\eta}\right\};$$

$$\underset{1\times12}{\left\{\Delta q^G\right\}^T}=\left\{\Delta q^i\ \ \Delta q^j\ \ \Delta q^k\ \ \Delta q^l\ \ \Delta q^i_{,a}\dots\Delta q^l_{,a}\ \ \Delta q^i_{,\beta}\dots\Delta q^l_{,\beta}\right\}.$$

Here, Δq means Δv^1, Δv^2 or Δv, and α and β are curvilinear global coordinates.

The functional (12) taking into account (8)–(11) and (13)–(16) can be transformed to the form:

$$\begin{aligned}\Phi_S=&\underset{1\times36}{\left\{\Delta U^G\right\}^T}\underset{36\times36}{\left[P_R\right]^T}\int\limits_F\underset{36\times6}{\left[B\right]^T}\underset{6\times1}{\left\{S^{\alpha\beta}\right\}^T}dF-\underset{1\times36}{\left\{\Delta U^G\right\}^T}\underset{36\times36}{\left[P_R\right]^T}\times\\ \times&\left(\int\limits_F\underset{36\times3}{\left[A\right]^T}\underset{3\times1}{\left\{P\right\}}dF-\frac{1}{2}\int\limits_F\underset{36\times3}{\left[A\right]^T}\underset{3\times1}{\left\{\Delta P\right\}}dF\right)+\frac{1}{2}\underset{1\times24}{\left\{\Delta S_u^{\alpha\beta}\right\}^T}\int\limits_F\underset{24\times6}{\left[H\right]^T}\underset{6\times6}{\left[\gamma\right]^{-1}}\underset{6\times24}{\left[H\right]}dF\underset{24\times1}{\left\{\Delta S_u^{\alpha\beta}\right\}}+\\ +&\underset{1\times24}{\left\{\Delta\varepsilon_{\alpha\beta u}\right\}^T}\frac{1}{2}\int\limits_F\underset{24\times6}{\left[H\right]^T}\underset{6\times6}{\left[\gamma\right]}\underset{6\times36}{\left[B\right]}dF\underset{36\times36}{\left[P_R\right]}\underset{36\times1}{\left\{\Delta U^G\right\}}-\underset{1\times24}{\left\{\Delta\varepsilon_{\alpha\beta u}\right\}^T}\frac{1}{2}\int\limits_F\underset{24\times6}{\left[H\right]^T}\underset{6\times24}{\left[H\right]}dF\underset{24\times1}{\left\{\Delta S_u^{\alpha\beta}\right\}}.\end{aligned}\tag{17}$$

For convenience of further calculations, we introduce the following matrix notations:

$$\begin{aligned}&\underset{24\times24}{\left[a\right]}=\int\limits_F\underset{24\times6}{\left[H\right]^T}\underset{6\times6}{\left[\gamma\right]^{-1}}\underset{6\times24}{\left[H\right]}dF;\quad \underset{24\times36}{\left[b\right]}=\frac{1}{2}\int\limits_F\underset{24\times6}{\left[H\right]^T}\underset{6\times6}{\left[\gamma\right]}\underset{6\times36}{\left[B\right]}dF\underset{36\times36}{\left[P_R\right]};\\ &\underset{24\times24}{\left[c\right]}=\frac{1}{2}\int\limits_F\underset{24\times6}{\left[H\right]^T}\underset{6\times24}{\left[H\right]}dF;\quad \underset{36\times1}{\left\{f_S\right\}}=\underset{36\times36}{\left[P_R\right]^T}\int\limits_F\underset{36\times6}{\left[B\right]^T}\underset{6\times1}{\left\{S^{\alpha\beta}\right\}}dF;\\ &\underset{36\times1}{\left\{f_p\right\}}=\underset{36\times36}{\left[P_R\right]^T}\int\limits_F\underset{36\times3}{\left[A\right]^T}\underset{3\times1}{\left\{P\right\}}dF;\quad \underset{36\times1}{\left\{f_{\Delta p}\right\}}=\underset{36\times36}{\left[P_R\right]^T}\int\limits_F\underset{36\times3}{\left[A\right]^T}\underset{3\times1}{\left\{\Delta P\right\}}dF.\end{aligned}\tag{18}$$

The functional (17) taking into account (18) can be written in the following form:

$$\begin{aligned}\Phi_S=&\underset{1\times36}{\left\{\Delta U^G\right\}^T}\underset{36\times1}{\left\{f_S\right\}}-\underset{1\times36}{\left\{\Delta U^G\right\}^T}\underset{36\times1}{\left\{f_p\right\}}-\frac{1}{2}\underset{1\times36}{\left\{\Delta U^G\right\}^T}\underset{36\times1}{\left\{f_{\Delta p}\right\}}+\\ +&\frac{1}{2}\underset{1\times24}{\left\{\Delta S_u^{\alpha\beta}\right\}^T}\underset{24\times24}{\left[a\right]}\underset{24\times1}{\left\{\Delta S_u^{\alpha\beta}\right\}}+\underset{1\times24}{\left\{\Delta\varepsilon_{\alpha\beta u}\right\}^T}\underset{24\times36}{\left[b\right]}\underset{36\times1}{\left\{\Delta U^G\right\}}-\underset{1\times24}{\left\{\Delta\varepsilon_{\alpha\beta u}\right\}^T}\underset{24\times24}{\left[c\right]}\underset{24\times1}{\left\{\Delta S_u^{\alpha\beta}\right\}}.\end{aligned}\tag{19}$$

By successively minimising (19) by $\left\{\Delta\varepsilon_{\alpha\beta u}\right\}^T$, $\left\{\Delta S_u^{\alpha\beta}\right\}^T$ and $\left\{\Delta U^G\right\}^T$, we can obtain the following system of matrix equations:

$$\begin{cases}\partial\Phi_S\Big/\partial\left\{\Delta\varepsilon_{\alpha\beta u}\right\}^T\equiv\underset{24\times36}{\left[b\right]}\underset{36\times1}{\left\{\Delta U^G\right\}}-\underset{24\times24}{\left[c\right]}\underset{24\times1}{\left\{\Delta S_u^{\alpha\beta}\right\}}=0;\\ \partial\Phi_S\Big/\partial\left\{\Delta S_u^{\alpha\beta}\right\}^T\equiv\underset{24\times24}{\left[a\right]}\underset{24\times1}{\left\{\Delta S_u^{\alpha\beta}\right\}}-\underset{24\times24}{\left[c\right]^T}\underset{24\times1}{\left\{\Delta\varepsilon_{\alpha\beta u}\right\}}=0;\\ \partial\Phi_S\Big/\partial\left\{\Delta U^G\right\}^T\equiv\underset{36\times1}{\left\{f_S\right\}}-\underset{36\times1}{\left\{f_p\right\}}-\underset{36\times1}{\left\{f_{\Delta p}\right\}}+\underset{36\times24}{\left[b\right]^T}\underset{24\times1}{\left\{\Delta\varepsilon_{\alpha\beta u}\right\}}=0.\end{cases}\tag{20}$$

To solve the system (20), we can use the substitution method. For this purpose, from the first and second equations (20), it is necessary to express the force and deformation step nodal unknowns:

$$\underset{24\times1}{\left\{\Delta S_u^{\alpha\beta}\right\}} = \underset{24\times24}{\left[c\right]}^{-1} \underset{24\times36}{\left[b\right]} \underset{36\times1}{\left\{\Delta U^G\right\}}; \quad \underset{24\times1}{\left\{\Delta\varepsilon_{\alpha\beta u}\right\}} = \left[\underset{24\times24}{\left[c\right]}^{T}\right]^{-1} \underset{24\times24}{\left[a\right]} \underset{24\times1}{\left\{\Delta S_u^{\alpha\beta}\right\}}. \tag{21}$$

By substituting (21) into the third equation (20), the following matrix equation can be obtained:

$$\underset{36\times1}{\left\{f_S\right\}} - \underset{36\times1}{\left\{f_p\right\}} - \underset{36\times1}{\left\{f_{\Delta p}\right\}} + \underset{36\times24}{\left[b\right]}^{T} \left[\underset{24\times24}{\left[c\right]}^{T}\right]^{-1} \underset{24\times24}{\left[a\right]} \underset{24\times24}{\left[c\right]}^{-1} \underset{24\times36}{\left[b\right]} \underset{36\times1}{\left\{\Delta U^G\right\}} = 0, \tag{22}$$

or in a more convenient form:

$$\underset{36\times36}{\left[K\right]} \underset{36\times1}{\left\{\Delta U^G\right\}} = \underset{36\times1}{\left\{f_{\Delta p}\right\}} - \left(\underset{36\times1}{\left\{f_S\right\}} - \underset{36\times1}{\left\{f_p\right\}}\right), \tag{23}$$

where $\underset{36\times36}{\left[K\right]} = \underset{36\times24}{\left[b\right]}^{T} \left[\underset{24\times24}{\left[c\right]}^{T}\right]^{-1} \underset{24\times24}{\left[a\right]} \underset{24\times24}{\left[c\right]}^{-1} \underset{24\times36}{\left[b\right]}$ is the stiffness matrix of the used four-node discretisation element of the three-field variant of the mixed FEM at one of the successive loading steps; $\underset{36\times1}{\left\{f_{\Delta p}\right\}}$ is the column of step forces; $\left(\underset{36\times1}{\left\{f_S\right\}} - \underset{36\times1}{\left\{f_p\right\}}\right)$ is the Newton–Raphson correction at the loading step.

To obtain the stiffness matrix of the finite element at the loading step, a numerical integration procedure was applied using the Gauss method for the area of the mid-surface $(n = 6)$ and the Simpson formula $(n = 7)$ when integrating over the shell thickness.

The global stiffness matrix of the shell structure $\left[K\right]$ is composed of a four-node discretisation element by means of an index matrix formed according to the accepted boundary conditions of the calculated shell [27].

In order to verify the above algorithm for the calculation of shell structures in a physically nonlinear formulation, a comparative analysis of finite element solutions obtained using the developed variant of the mixed FEM with the solutions obtained on the basis of the FEM in the formulation of the displacement method was performed.

3. Results and Discussion

Example 1. As an example, a fragment of an elliptical cylinder made of duralumin alloy with the ratio of ellipse parameters of cross-section a/b = 5, loaded with internal pressure of intensity q = 6·10^{-3} MPa, was calculated. The calculation scheme of the shell is shown in Fig. 1. The following initial data were used: a = 1.5 m; b = 0.3 m; h = 0.01 m; L = 0.01 m; E = 7.49·10^4 MPa; ν = 0.32. The deformation diagram was assumed as a two-linked broken line defined by the formula:

$$\begin{cases} \sigma_i = tg\alpha \cdot \varepsilon_i; & \varepsilon_i \le 0.0023496; \\ \sigma_i = tg\beta \cdot \left(\varepsilon_i - 0.0023496\right) + 200; & \varepsilon_i > 0.0023496, \end{cases}$$

where $\mathrm{tg}\alpha = 85120.87;\ \mathrm{tg}\beta = 18087.03.$

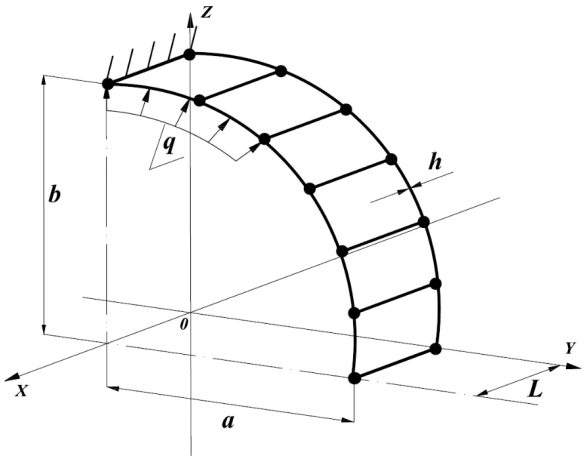

Figure 1. Calculation diagram of an elliptical cylinder.

The calculations were performed in two variants: in the first variant, the above three-field mixed FEM algorithm in a physically nonlinear formulation was implemented; in the second variant, the FEM algorithm in the formulation of the displacement method was used. The results of the variant calculations are presented in tabular form. The tables show the numerical values of normal stresses in the rigid embedment and at the free end of the shell, as well as the values of bending moment (for the first variant of calculation) when varying the degree of refinement of the discretisation grid and the number of loading steps.

Tables 1–3 present the results of the first variant of calculation at successive densification of the mesh of nodes 41×2, 51×2, and 61×2 depending on the number of stages of successive loading.

The selected design scheme allows to calculate the values of physical bending moment in the rigid embedment (Fig. 2):

$$M_{22} = \left(q_{\text{в}} b^2 / 2 + q_{\text{г}} c^2 / 2\right) L = \left(q/2\right)\left(b^2 + c^2\right) L =$$

$$= 3 \cdot 10^3 \ \text{N}/\text{m}^2 \cdot \left(\left(1.5\text{m}\right)^2 + \left(0.3\text{m}\right)^2\right) \cdot 10^{-2}\,\text{m} = 3 \cdot 10 \cdot 2.34 \ \text{N} \cdot \text{m} = 70.2 \ \text{N} \cdot \text{m}.$$

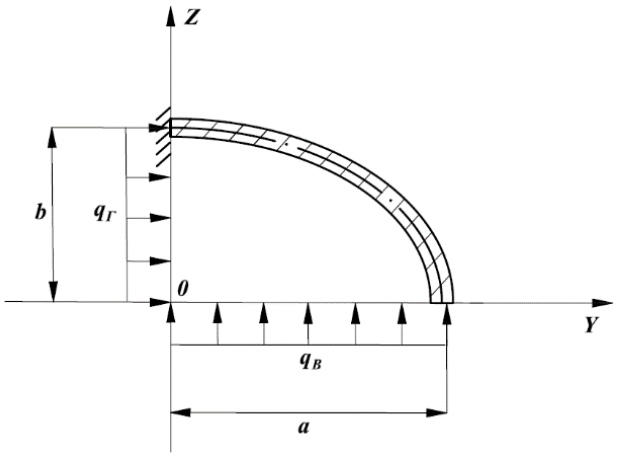

Figure 2. Section of the shell by the plane ZOY.

It is also obvious that the bending moment M_{22} at the free end of the elliptical cylinder, as well as the stresses, must be equal to zero.

The rightmost column of Tables 1–3 shows the above-mentioned analytical values of the controlled strength parameters of the shell SSS.

Table 1. Values of controlled SSS parameters at 41×2 node grid.

Point coordinates, *y*, m; *z*, m	Stress σ, MPa, moment, M_{22}, N·m	Number of loading steps				Analytical solution
		22	52	82	102	
0.0; 0.3	σ_{22}^{in}	347.3	347.5	347.6	347.6	–
	σ_{22}^{out}	-346.7	–347.1	–347.1	–347.1	–
	M_{22}	70.74	70.55	70.22	70.16	70.20
1.5; 0.0	σ_{22}^{in}	–0.192	–0.190	–0.190	–0.191	–
	σ_{22}^{out}	–0.137	–0.136	–0.136	–0.136	–
	σ_{22}^{midl}	0.0687	0.0681	0.0681	0.0685	0.000
	M_{22}	0.0005	0.0005	0.0005	0.0005	0.000

Table 2. Values of controlled SSS parameters at 51×2 node grid.

Point coordinates, *y*, m; *z*, m	Stress σ, MPa, moment, M_{22}, N·m	Number of loading steps				Analytical solution
		22	52	82	102	
0.0; 0.3	σ_{22}^{in}	347.4	347.6	347.6	347.6	–
	σ_{22}^{out}	–346.7	–347.1	-347.2	–347.2	–
	M_{22}	70.87	70.36	70.32	70.29	70.20
1.5; 0.0	σ_{22}^{in}	–0.0708	–0.0682	–0.0679	–0.0683	–
	σ_{22}^{out}	–0.0533	–0.0514	–0.0511	–0.0515	–
	σ_{22}^{midl}	0.0273	0.0266	0.0265	0.0266	0.000
	M_{22}	0.0004	0.0004	0.0004	0.0004	0.000

Table 3. Values of controlled SSS parameters at 61×2 node grid.

Point coordinates, *y*, m; *z*, m	Stress σ, MPa, moment, M_{22}, N·m	Number of loading steps				Analytical solution
		22	52	82	102	
0.0; 0.3	σ_{22}^{in}	347.5	347.6	347.7	347.7	–
	σ_{22}^{out}	–346.7	–347.1	–347.2	–347.2	–
	M_{22}	71.03	70.50	70.37	70.33	70.20
1.5; 0.0	σ_{22}^{in}	–0.0295	–0.0298	–0.0299	–0.0297	–
	σ_{22}^{out}	–0.0223	–0.0225	–0.0225	–0.0224	–
	σ_{22}^{midl}	0.0119	0.0120	0.0120	0.0120	0.000
	M_{22}	0.0003	0.0003	0.0003	0.0003	0.000

As follows from the analysis of the data given in Tables 1–3, the three-field version of the mixed FEM in the physically nonlinear formulation demonstrates stable convergence of the computational process, both when the discretisation grid is reduced and when the number of successive loading stages is increased. In addition, the numerical values of the bending moment M_{22} in the rigid embedment and at the free end practically coincide with their analytical values, which is also a proof of the correctness and high degree of

accuracy of finite element solutions obtained by using the developed three-field mixed FEM in the physically nonlinear formulation.

If the classical FEM formulation of the displacement method is applied to the solution of this problem, the results of finite element solutions will be quite different from the above-mentioned ones. For example, Table 4 shows the results of the FEM calculation of an elliptical cylinder in the form of the displacement method with a 61×2 node grid.

Table 4. Stress values of elliptical cylinder FEM in the form of displacement method with 61×2 node grid.

Point coordinates, *y*, m; *z*, m	Stress σ_{22}, MPa	Number of loading steps				Analytical solution
		22	52	82	102	
0.0; 0.3	σ_{22}^{in}	304.1	274.6	120.3	276.0	–
	σ_{22}^{out}	–303.8	–274.3	–112.7	–275.8	–
1.5; 0.0	σ_{22}^{in}	–76.44	–66.17	–140.8	–62.41	–
	σ_{22}^{out}	358.4	323.2	330.2	319.4	–
	σ_{22}^{midl}	270.7	250.8	246.4	248.9	0.000

As follows from the analysis of Table 4, there is no convergence of the computational process when the number of successive loading steps is increased. In addition, the stresses at the free end of the shell reach unacceptably high values, although they should be equal to zero.

Obviously, when using the FEM in the formulation of the displacement method in physically nonlinear calculations of shells with significant curvature of the medial surface, a much more significant refinement of the discretisation grid is required. Tables 5–7 show the results of elliptical cylinder calculations with 81×2, 101×2, and 121×2 node grids, respectively.

Table 5. Stress values of elliptical cylinder FEM in the form of displacement method with 81×2 node grid.

Point coordinates, *y*, m; *z*, m	Stress σ_{22}, MPa	Number of loading steps				Analytical solution
		22	52	82	102	
0.0; 0.3	σ_{22}^{in}	343.9	302.9	369.0	264.1	–
	σ_{22}^{out}	–343.4	–302.2	–370.4	–263.0	–
1.5; 0.0	σ_{22}^{in}	–66.74	–59.54	–32.91	–56.99	–
	σ_{22}^{out}	278.5	259.7	253.6	248.7	–
	σ_{22}^{midl}	213.8	178.8	176.7	156.3	0.000

Table 6. Stress values of elliptical cylinder FEM in the form of displacement method with 101×2 node grid.

Point coordinates, *y*, m; *z*, m	Stress σ_{22}, MPa	Number of loading steps				Analytical solution
		22	52	82	102	
0.0; 0.3	σ_{22}^{in}	345.0	345.2	344.2	341.6	–
	σ_{22}^{out}	–344.5	–344.8	–343.8	–341.2	–
1.5; 0.0	σ_{22}^{in}	–47.34	–47.49	–47.21	–46.41	–
	σ_{22}^{out}	227.5	227.7	227.2	225.6	–
	σ_{22}^{midl}	114.9	115.2	114.6	112.9	0.000

Table 7. Stress values of elliptical cylinder FEM in the form of displacement method with

121×2 node grid.

Point coordinates, *y*, m; *z*, m	Stress σ_{22}, MPa	Number of loading steps				Analytical solution
		22	52	82	102	
0.0; 0.3	σ_{22}^{in}	346.3	346.6	346.6	346.6	–
	σ_{22}^{out}	–345.8	–346.1	–346.1	–346.1	–
1.5; 0.0	σ_{22}^{in}	–37.30	–37.41	–37.43	–37.44	–
	σ_{22}^{out}	145.1	145.6	145.7	145.8	–
	σ_{22}^{midl}	69.49	69.74	69.80	69.81	0.000

Analysing the tabulated values of normal stresses in Table 5 shows that for 81×2 node grid, there is also no convergence of the computational process as the number of sequential loading steps increases and the stresses at the free end have unacceptably high values.

For 101×2 node grid in rigid embedment (Table 6), satisfactory convergence of the computational process is observed. However, the stresses at the free end have unacceptably high values.

With a 121×2 node grid (Table 7), the values of stresses in the rigid embedment remain almost unchanged and coincide with the values of stresses in the rigid embedment obtained using the three-field version of mixed FEM (Tables 1–3). However, at the free end, the normal stresses still remain very far from zero values, which requires further refinement of the discretisation grid.

Table 8 shows the calculation results of the elliptical cylinder at 201×2 node grid. As can be seen from the analysis of the tabular data, a steady convergence of the computational process is observed in the rigid termination as the number of successive loading steps increases. At the free end of the shell, the stress values have decreased but still remain quite far from zero values.

Table 8. Stress values of elliptical cylinder FEM in the form of displacement method with 201×2 node grid.

Point coordinates, *y*, m; *z*, m	Stress σ_{22}, MPa	Number of loading steps				Analytical solution
		22	52	82	102	
0.0; 0.3	σ_{22}^{in}	347.2	347.5	347.6	347.6	–
	σ_{22}^{out}	–346.8	–347.0	–347.1	–347.1	–
1.5; 0.0	σ_{22}^{in}	–17.44	–17.49	–17.50	–17.51	–
	σ_{22}^{out}	40.28	40.41	40.44	40.45	–
	σ_{22}^{midl}	16.31	16.37	16.38	16.38	0.000

In addition, it should be noted that when using the traditional formulation of the FEM in the form of the displacement method, the problem of obtaining the numerical value of the bending moment in the rigid embedment arises. To solve this problem, a graphical method can be applied to calculate the bending moment value from the normal stress epiphysis in the rigid embedment, plotted at fixed points of vertical coordinate along the normal to the medial surface of the shell.

Fig. 3 shows the normal stress epiphysis in the rigid embedment with a 201×2 node grid plotted at 9 node points along the surface normal. For convenience of further calculations, the epyure was divided into elementary figures and the centres of gravity in each figure were found. Then, the forces $\vec{T}_i \left(i = 1,\ldots,10\right)$ were calculated as the areas of each of the figures. Moments were calculated as products of forces by the corresponding arms $\vec{M}_i = \vec{T}_i \cdot d_i \left(i = 1,\ldots,10\right)$.

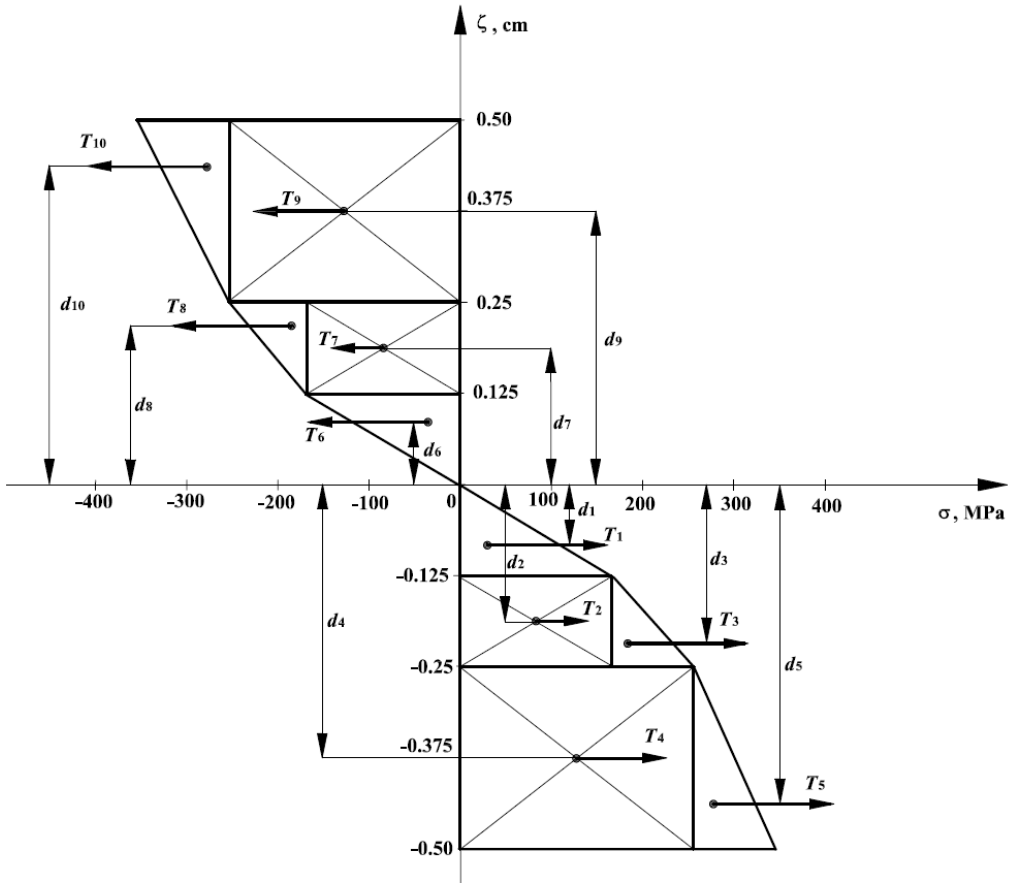

Figure 3. Normal stress diagram in a rigid termination.

The resultant moment can be obtained by summing the moments $\vec{M}_i$:

$$M_{22} = \sum_{i=1}^{10} \left| \vec{M}_i \right|.$$

After performing the above calculations, the resultant torque is obtained as follows:

$$M_{22} = 69.554 \text{ N} \cdot \text{m}.$$

The calculation error was:

$$\delta = \frac{70.2 - 69.554}{70.2} \cdot 100\% = 0.92\%.$$

Obviously, when building a more detailed stress diagram, for example, by dividing it by height into 17 points, the calculation error can be reduced. However, the error of 0.92 % obtained by dividing the stress diagram into 9 points along the section height is quite acceptable for engineering calculations.

Calculation example 2: A fragment of an elliptical ring with the ratio of ellipse parameters a/b = 6, loaded on the right side with a linear load of intensity q = 25 kN/m uniformly distributed along the formations and having a hinged support on the left side, was calculated (Fig. 4). The following initial data were used: a = 1.2 m; b = 0.2 m; h = 0.008 m; L = 0.01 m. The physical characteristics of the material and the deformation diagram were taken from the previous calculation example. A reactive force equal to the applied nodal load occurs at the hinge points $R = Q$. Thus, the normal stresses σ_{22} at points K and M must be equal. The equality of the normal stresses σ_{22} at points K and M can serve as an additional criterion for the correctness of the numerical values of the normal stresses obtained as a result of the solution.

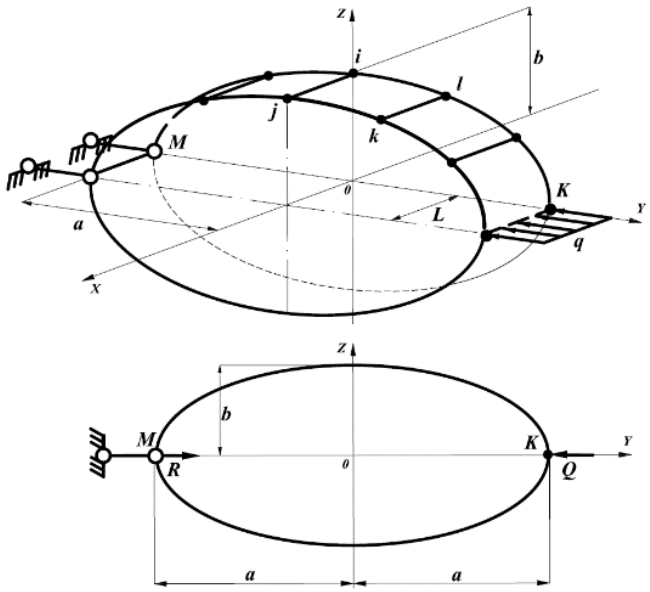

Figure 4. Calculation diagram of an elliptical ring.

The calculations, as in the previous example, were performed in two variants: the first variant used the developed three-field mixed four-node discretisation element; the second variant used a finite element whose stiffness matrix was composed in the formulation of the displacement method. The results of the first variant of the calculation are summarised in Tables 9 and 10. Table 9 shows the values of normal stresses on the inner and outer surfaces of the shell at the points of application of a given load and at the points of hinge support depending on the density of the discretisation grid at a fixed number of loading steps equal to 22.

Table 9. Stress values of the first calculation variant depending on the size of the discretisation grid.

Point coordinates, *y*, m; *t*, m	Stress σ_{22}, MPa	Sampling grid			
		51×2	61×2	81×2	101×2
1.2; π/2	σ_{22}^{in}	303.5	304.0	305.2	305.5
	σ_{22}^{out}	–270.1	–270.4	–271.0	–271.2
–1.2; π/2	σ_{22}^{in}	303.0	304.0	305.2	305.5
	σ_{22}^{out}	–269.6	–270.3	–271.0	–271.1

Analysis of the data shown in Table 9 indicates the stable convergence of the computational process as the discretisation grid thickens and the values of normal stresses at points K and M practically coincide, which should be the case with the selected design scheme.

Table 10 shows the results of the shell calculation with a fixed discretisation grid of 61×2 and a sequential increase in the number of sequential loading stages.

Table 10. Stress values of the first variant depending on the number of loading steps.

Point coordinates, *y*, m; *t*, m	Stress σ_{22}, MPa	Number of loading steps			
		22	52	82	102
1.2; π/2	σ_{22}^{in}	304.0	304.7	304.8	304.8
	σ_{22}^{out}	–270.4	–270.5	–270.6	–270.55
–1.2; π/2	σ_{22}^{in}	304.0	304.7	304.8	304.8
	σ_{22}^{out}	–270.3	–270.4	–270.4	–270.4

As follows from the analysis of the data in Table 10, a stable convergence of the computational process is observed. The numerical values of normal stresses change very slightly when the number of loading steps increases from 22 to 102, which is also a necessary condition for the reliability of the numerical values of stresses obtained as a result of the calculation.

The results of calculations for the second variant, in which the FEM algorithm in the classical formulation of the displacement method was implemented, are presented in Tables 11 and 12. Table 11 contains the results of calculations with a fixed number of loading steps equal to 22 and successive densification of the discretisation grid from 61×2 to 201×2.

Table 11. Stress values of the second calculation variant depending on the size of the discretisation grid.

Point coordinates, *y*, m; *t*, m	Stress σ_{22}, MPa	Sampling grid					
		61×2	81×2	101×2	121×2	151×2	201×2
1.2; π/2	σ_{22}^{in}	711.6	528.7	442.5	394.8	357.8	334.4
	σ_{22}^{out}	–284.7	–320.9	–319.0	–309.5	–297.7	–287.5
–1.2; π/2	σ_{22}^{in}	276.9	301.7	301.1	302.9	305.9	305.7
	σ_{22}^{out}	–250.1	–269.1	–268.1	–269.5	–271.6	–271.4

The analysis of Table 11 shows a very slow convergence of the computational process as the discretisation grid of the calculated shell becomes denser. It can also be noted that the normal stresses σ_{22} at the load application points q and the hinge points do not match. Fig. 5 shows a plot of the variation of the stress ratio $k = \left(\sigma_{22}^{in}\right)_K \Big/ \left(\sigma_{22}^{in}\right)_M$ at the K and M points of the shell as a function of the density of the discretisation grid in the two computational formulations of the FEM.

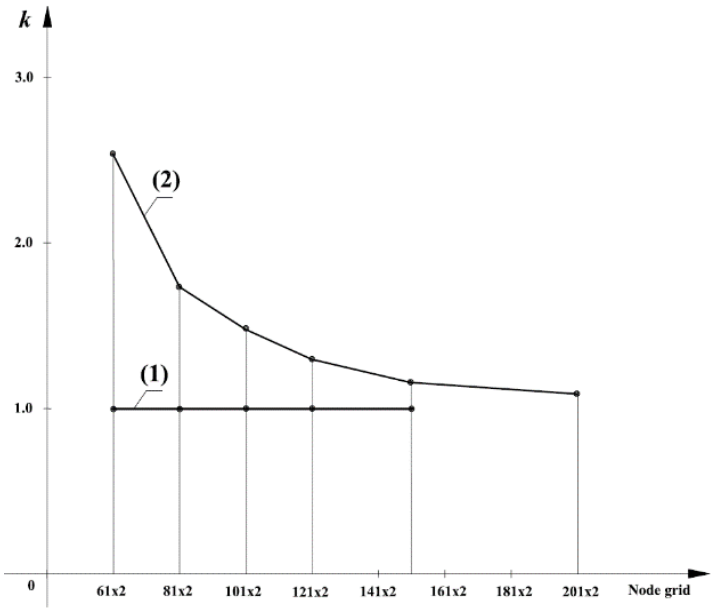

Figure 5. Plots of coefficient *k* variation depending on the size of the sampling grid for the first (1) and second (2) variants of calculation for the first (1) and the second (2) calculation variants.

As can be seen from Fig. 5, the developed three-field mixed FEM algorithm allows to have a coefficient k equal to 1 at any, even very sparse, discretisation grid, whereas the FEM in the formulation of the displacement method does not allow to achieve such a result, despite a very significant densification of the discretisation grid. Further densification of the mesh is also not reasonable, as it leads to the accumulation of rounding errors at the size of the discretisation element comparable to its thickness, which does not meet the criteria of a thin shell.

Table 12 shows the results of the second variant of calculation at a fixed 201×2 discretisation grid depending on the number of stages of sequential loading.

Table 12. Stress values of the second variant depending on the number of loading steps.

Point coordinates, *y*, m; *t*, m	Stress σ_{22}, MPa	Number of loading steps			
		22	52	82	102
1.2; π/2	σ_{22}^{in}	334.4	313.1	318.5	311.7
	σ_{22}^{out}	–287.5	–271.6	–276.4	–271.1
–1.2; π/2	σ_{22}^{in}	305.7	295.1	285.7	282.4
	σ_{22}^{out}	–271.4	–263.4	–256.6	–254.1

As follows from the analysis of the data in Table 12, satisfactory convergence of the computational process is observed, but the difference between the stress values at points K and M remains almost constant within 10 %, which should not be the case with the selected design scheme.

Calculation example 3. A calculation was made of a truncated ellipsoid of revolution under the action of internal pressure of intensity q = 6.5 MPa (Fig. 6). The left end was rigidly clamped, the right end was free. The geometric dimensions of the ellipsoid were taken to be: a = 1.3 m; b = 0.8 m; h = 0.02 m; coordinate x was determined by inequality $0 \le x \le 1.2$ m. The physical properties of the shell material were taken from the previous example. Considering that the right free end of the ellipsoid is in a momentless state, the value of the normal stress in the hoop stress can be found using the Laplace formula [28]

$$\sigma_{xx}/R_x + \sigma_{tt}/R_t = q/h.$$

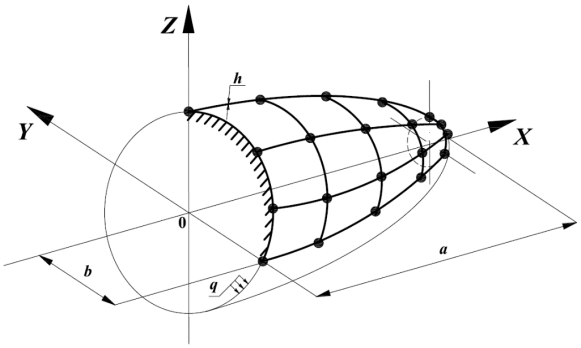

Figure 6. Calculation scheme of an ellipsoidal shell.

Taking into account that on the free end σ_{xx} should be equal to zero, σ_{tt}^{midl} will be equal:

$$\sigma_{tt}^{midl} = (q/h)\cdot R_t = (6.5\ \text{MPa}/0.02\ \text{m})\cdot 0.5488\ \text{m} = 178.36\ \text{MPa}.$$

During the solution process, the convergence of the computational process was monitored both as the mesh density increased and as the number of loading steps increased. Table 13 presents the stress values on the internal σ^{in}, external σ^{out} and median σ^{midl} the ellipsoid surfaces at the supporting and free ends, depending on the degree of mesh density for a fixed number of loading steps equal to 22.

The stress calculated using the Laplace formula is included in the far right column of Table 13.

Table 13. Stress values depending on the discretization grid size.

Shell cross-section	Stress σ, MPa	Sampling grid				Analytical solution
		201×21	301×21	361×21	401×21	
Support, *x* = 0.0 m	σ_{xx}^{in}	322.3	327.2	324.2	326.1	–
	σ_{xx}^{out}	–232.4	–236.5	–233.8	–233.9	–
	σ_{xx}^{midl}	162.7	164.4	163.4	165.1	–

Shell cross-section	Stress σ, MPa	Sampling grid				Analytical solution
		201×21	301×21	361×21	401×21	
Free end, x = 1.2 m	σ_{xx}^{in}	0.073	0.035	0.033	0.034	–
	σ_{xx}^{out}	0.068	0.033	0.030	0.031	–
	σ_{xx}^{midl}	0.062	0.025	0.022	0.024	0.00
	σ_{tt}^{in}	182.7	183.0	184.2	185.4	–
	σ_{tt}^{out}	169.9	170.2	171.4	172.6	–
	σ_{tt}^{midl}	176.14	176.44	177.61	178.86	178.36

Analyzing the data presented in Table 13, we can confirm stable convergence of the calculations and consider a 201×21 node grid to be entirely sufficient.

Table 14 shows the values of the controlled parameters of the ellipsoid SSS for a 201×21 node grid depending on the number of loading steps.

Table 14. Stress values depending on the number of loading steps.

Shell cross-section	Stress σ, MPa	Number of loading steps				Analytical solution
		22	32	42	52	
Support, x = 0.0 m	σ_{xx}^{in}	322.3	320.3	320.1	320.4	–
	σ_{xx}^{out}	–232.4	–231.1	–231.0	–230.9	–
	σ_{xx}^{midl}	162.7	161.3	161.1	161.8	–
Free end, x = 1.2 m	σ_{xx}^{in}	0.073	0.074	0.082	0.083	–
	σ_{xx}^{out}	0.068	0.068	0.075	0.076	–
	σ_{xx}^{midl}	0.062	0.062	0.070	0.071	–
	σ_{tt}^{in}	182.7	182.8	183.5	183.6	–
	σ_{tt}^{out}	169.9	170.0	170.7	170.8	–
	σ_{tt}^{midl}	176.14	176.21	176.92	177.02	178.36

Table 14 shows that as the number of loading steps increases, the stress values change only slightly. Therefore, the stability of the computational process convergence is ensured. The numerical stresses at the free end of the ellipsoid correspond to their analytical values with an acceptable error of 0.75 %.

The multipolic end-element approach to the analysis of the elastoplastic deformation was used in works [25, 28–31], in which in addition to the fields of displacements and stresses, additional fields of plastic factors were used in expressions to determine the speeds of plastic deformations.

In this work, in the mixed formulation of the FEM, they are used as the desired fields of unknown quantities: increment of movements, deformations and curvatures of the midlife, as well as increment of efforts and moments.

To obtain a plasticity matrix, a deformation theory of plasticity [4] is realized in a step of loading, which made it possible to exclude an additional field of unknowns – the field of plastic factors.

4. Conclusions

1. A nonlinear mixed functional with three fields of step unknowns: kinematic, force and strain is proposed.
2. Based on the proposed nonlinear mixed functional, an algorithm for forming the stiffness matrix of a curvilinear four-node discretisation element at a loading step is developed.

3. A comparative analysis of finite element solutions obtained using the developed algorithm and solutions obtained on the basis of single-field FEM in the formulation of the displacement method has been performed.
4. The analysis of the results of the comparative analysis proved the significant advantages of the developed three-field FEM in the calculation of shell structures in the physically nonlinear formulation in comparison with the single-field FEM in the form of the displacement method.

References

1. Sedov, L.I. Mekhanika sploshnoy sredy [Mechanics of a continuous medium]. 1. Moscow: Nauka, 1976. 536 p.
2. Zubchaninov, V.G. Mekhanika sploshnykh deformiruyemykh sred [Mechanics of continuous deformable media]. Tver: TSTU, 2000. 703 p.
3. Petrov, V.V., Krivoshein, I.V. Metody rascheta konstruktsiy iz nelineyno deformiruyemogo materiala [Methods for calculating structures made of nonlinearly deformable material]. Moscow: ASV Publishing House, 2009. 208 p.
4. Malinin, N.N. Prikladnaya teoriya plastichnosti i polzuchesti [Applied theory of plasticity and creep]. Moscow: Yurayt Publishing House, 2024. 402 p.
5. Paimushin, V.N. Nonlinear Theory of Sandwich Shells with a Transversely Soft Core Containing Delamination Zones and Edge Support Diaphragm. Mechanics of Solids. 2018. 53(1). Pp. 76–87. DOI: 10.3103/S0025654418030111
6. Bazhenov, V.G., Kazakov, D.A., Osetrov, S.L., Osetrov, D.L., Ryabov, A.A. Analysis of the Limiting States of Cylindrical Elastic-Plastic Shells under Tension and Combined Loading by Internal Pressure and Tension. PNRPU Mechanics Bulletin. Mechanics. 2022. 2. Pp. 39–48. DOI: 10.15593/perm.mech/2022.2.04
7. Bazhenov, V.G., Kazakov, D.A., Kibets, A.I., Nagornykh, E.V., Samsonova, D.A. Formulation and Numerical Solution of the Stability Loss Problem of Elastic-Plastic Shells of Revolution with an Elastic Filler under Combined Axisymmetric and Torsional Loadings. PNRPU Mechanics Bulletin. 2022. 3. Pp. 95–106. DOI: 10.15593/perm.mech/2022.3.10
8. Levin, V.A., Vershinin, A.V. Nelineynaya vychislitel'naya mekhanika prochnosti [Nonlinear computational strength mechanics]. 2: Numerical methods [Chislennyye metody]. Moscow: Fizmatlit, 2015. 544 p.
9. Levin, V.A. Nelineynaya vychislitel'naya mekhanika prochnosti [Nonlinear computational strength mechanics]. 1: Modeli i metody [Models and methods]. Moscow: Fizmatlit, 2015. 456 p.
10. Madeo, A., Liguori, F., Zucco, G., Fiore, S. An efficient isostatic mixed shell element for coarse mesh solution. International Journal for Numerical Methods in Engineering. 2021. 122(1). Pp. 82–121. DOI: 10.1002/nme.6526
11. Cavalcante, E., Neto, E.L. A pseudo-equilibrium finite element for limit analysis of Reissner-Mindlin plates. Applied Mathematical Modelling. 2021. 96. P. 336–354. DOI: 10.1016/j.apm.2021.03.004
12. Sagdatullin, M.K. Numerical Modeling of Nonlinear Deformation Processes for Shells of Medium Thickness. Structural mechanics of engineering constructions and buildings. 2023. 19(2). Pp. 130–148. DOI: 10.22363/1815-5235-2023-19-2-130-148
13. Sultanov, L.U. Analysis of Finite Elasto-Plastic Strains: Integration Algorithm and Numerical Examples. Lobachevskii Journal of Mathematics. 2018. 39(9). Pp. 1478–1483. DOI: 10.1134/S1995080218090056
14. Golovanov, A.I., Tyuleneva, O.N., Shigabutdinov, A.F. Metod konechnykh elementov v statike i dinamike tonkostennykh konstruktsiy [Finite element method in the statics and dynamics of thin-walled structures]. Moscow: Fizmatlit., 2006. 391 p.
15. Khairullin, F.S., Sakhbiev, O.M. Calculation of the Elastoplastic Deformations by the Variational Method Based on Functions with Finite Carriers. Herald of Technological University. 2021. 24(4). Pp. 102–106.
16. Klochkov, Yu.V., Pshenichkina, V.A., Nikolaev, A.P., Marchenko, S.S., Vakhnina, O.V., Klochkov, M.Yu. Calculation of Shells of Revolution with the Use of a Mixed FEM with a Vector Approximation Procedure. Journal of Machinery Manufacture and Reliability. 2024. 52(1). Pp.10–21. DOI: 10.1134/S1052618824010059
17. Cervera, M., Chiumenti, M., Codina, R. Mixed stabilized finite element methods in nonlinear solid mechanics: Part I: Formulation. Computer Methods in Applied Mechanics and Engineering. 2010. 199(37–40). Pp. 2559–2570. DOI: 10.1016/j.cma.2010.04.006
18. Nodargi, N.A., Bisegna, P. A novel high-performance mixed membrane finite element for the analysis of inelastic structures. Computers & Structures. 2017. 182. Pp. 337–353. DOI: 10.1016/j.compstruc.2016.10.002
19. Liguori, F.S., Madeo, A., Garcea, G. A mixed finite-element formulation for the elasto-plastic analysis of shell structures. Materials Research Proceedings. 2023. 26. Pp. 227–232. DOI: 10.21741/9781644902431-37
20. Liguori, F.S., Madeo, A., Garcea, G. A dual decomposition of the closest point projection in incremental elasto-plasticity using a mixed shell finite element. International Journal for Numerical Methods in Engineering. 2022. 123(24). Pp. 6243–6266. DOI: 10.1002/nme.7112
21. Bilotta, A., Garcea, G., Leonetti, L. A composite mixed finite element model for the elasto-plastic analysis of 3D structural problems. Finite Elements in Analysis and Design. 2016. 113. Pp. 43–53. DOI: 10.1016/j.finel.2016.01.002
22. Mendes, L.A.M., Castro, L.M.S.S. Hybrid-mixed stress finite element models in elastoplastic analysis. Finite Elements in Analysis and Design. 2009. 45(12). Pp. 863–875. DOI: 10.1016/j.finel.2009.06.021
23. Madeo, A., Liguori, F., Zucco, G. et al. An efficient isostatic mixed shell element for coarse mesh solution. International Journal for Numerical Methods in Engineering. 2021. 122(1). Pp. 82–121. DOI: 10.1002/nme.6526
24. Klochkov, Yu., Nikolaev, A., Pshenichkina, V., Vakhnina, O., Klochkov, M. Three-field FEM for analysis of thin elastic shells. Magazine of Civil Engineering. 2024. 3(127). Article no. 12710. DOI: 10.34910/MCE.127.10
25. Bilotta, A., Leonetti, L., Garcea, G. Three field finite elements for the elastoplastic analysis of 2D continua. Finite Elements in Analysis and Design. 2011. 47(10). Pp. 1119–1130. DOI: 10.1016/j.finel.2011.05.002
26. Novozhilov, V.V. Teoriya tonkikh obolochek [Theory of thin shells]. St. Petersburg: Publishing House of the St. Petersburg University, 2010. 378 p.
27. Postnov, V.A., Kharkhurim, I.Ya. Metod konechnykh elementov v raschetakh sudovykh konstruktsiy [Finite element method in calculations of ship structures]. Leningrad: Sudostroyeniye, 1974. 342 p.
28. Belyaev, N.M. Soprotivleniye materialov [Strength of materials]. Moscow: Nauka, 1976. 607 p.

29. Nodargi, N.A. An Overview of Mixed Finite Elements for the Analysis of Inelastic Bidimensional Structures. Archives of Computational Methods in Engineering. 2019. 26. Pp. 1117–1151. DOI: 10.1007/s11831-018-9293-0
30. Simo, J.C, Kennedy, J.G, Taylor, R.L. Complementary mixed finite element formulations for elastoplasticity. Comput. Methods Appl Mech Eng. 1989. 74(2). Pp. 177–206. DOI: 10.1016/0045-7825(89)90102-3
31. Arnold, D.N., Boffi, D., Falk, R.S. Approximation by quadrilateral finite elements. Mathematics of Computation. 2002. 71(239). Pp. 909–922. DOI: 10.1090/S0025-5718-02-01439-4

Information about the authors:

Mikhail Klochkov,
ORCID: https://orcid.org/0000-0001-6751-4629
E-mail: m.klo4koff@yandex.ru

Valeria Pshenichkina, *Doctor of Technical Sciences*
ORCID: https://orcid.org/0000-0001-9148-2815
E-mail: vap_hm@list.ru

Anatoly Nikolaev, *Doctor of Technical Sciences*
ORCID: https://orcid.org/0000-0002-7098-5998
E-mail: anpetr40@yandex.ru

Yuri Klochkov, *Doctor of Technical Sciences*
ORCID: https://orcid.org/0000-0002-1027-1811
E-mail: klotchkov@bk.ru

Olga Vakhnina, *PhD in Technical Sciences*
ORCID: https://orcid.org/0000-0001-9234-7287
E-mail: ovahnina@bk.ru

Received 17.05.2025. Approved after reviewing 03.02.2026. Accepted 03.02.2026.